Propagation Theory

Charles Rino

January 22, 2019

Abstract

This informal report is intended to be one of a series of that review recent developments in diagnostic propagation measurements stimulated by the global navigation satellite system. The equivalent phase screen model is particularly appealing because it is supported by a complete theory and evolving diagnostic applications to real data. The report introduces a *GNSS Propagation Toolbox* of MatLab utilities and supporting libraries that will generate the theoretical results and supporting phase-screen simulations.

We should nonetheless keep in mind that the results are based on statistical phase-screen equivalence and extraction of representative one-dimensional scans. New results that address these issues are referenced.

1 Introduction

For the purposes of this topical review propagation theory will refer to the propagation of electromagnetic (EM) waves in transparent structured media. Transparent media are characterized by a continuous refractive index with a negligibly small imaginary component. EM fields are vectors that vary in both space and time. Spatial variation is captured by frequency-domain (time-harmonic) analysis. The scalar form of the time-harmonic propagation equations characteriz the horizontal electric field component, which captures the essential scintillation structure. A complete development can be found in Chapters 1 and 2 of Rino [1].

The flow of energy in a transparent medium follows a prescribed path predominantly away from the source, which leads to the forward approximation. Under the forward approximation the EM field is unaffected by small amounts of energy scattered back toward the source. The theory includes refraction, which is an approximation captured by ray tracing, and diffraction, which accounts for local field enhancements and cancellation. The term scattering is reserved for electromagnetic wave interactions with objects that have definitive boundaries.

The theoretical development starts with the specification of a reference coordinate system. Plane-wave decompositions require rectangular reference coordinate systems. Detailed structure computations are necessarily confined to

regions of interest (ROIs) as described in a separate ionospheric structure model (ISM) review. Propagation calculations are acutely sensitive to the reference coordinate system. For example, scattering from a rough surface generally favors a principal reference coordinate normal to the surface, whereas point-to-point propagation between a near-earth transmitter and receiver favors earth-parallel propagation. An inverted topocentric coordinate system was used in Rino [1] for satellite-to-earth propagation calculations. The propagation geometry identifies local ROIs. An example can be found in [2]. However, the downward orientation of the propagation reference eliminates occultation geometries. To avoid such problems this review will use a coordinate system with the principal axis along the propagation direction. There is no loss of generality, although the vector pointing along the magnetic field must be computed in the field-aligned coordinate system. The complementary fixed and propagation-aligned coordinate system choices stem from early seminal papers by K. B. Budden [3] and by Briggs and Parkin [4].

For propagation diagnostics and simulations a scalar wavefield, $\psi\left(x,\boldsymbol{\rho};f\right)$, that represents one frequency component of a satellite-to-earth transmission will suffice. For notational simplicity the frequency dependence will be left implicit. The forward propagation equation (FPE)

$$\frac{\partial\psi\left(x,\boldsymbol{\rho}\right)}{\partial x}=\Theta\psi\left(x,\boldsymbol{\rho}\right)+ik\Delta n\left(x,\boldsymbol{\rho}\right)\psi\left(x,\boldsymbol{\rho}\right), \tag{1}$$

governs propagation in a structured transparent medium. The wavefield $\psi\left(x,\boldsymbol{\rho}\right)$ at x can be decomposed into two-dimensional Fourier components

$$\widehat{\psi}\left(x,\boldsymbol{\kappa}\right)=\iint\psi\left(x,\boldsymbol{\rho}\right)\exp\{-i\boldsymbol{\kappa}\cdot\boldsymbol{\rho}\}d\boldsymbol{\rho}$$

The wave vector

$$\mathbf{k}=[k_x,\boldsymbol{\kappa}], \tag{2}$$

characterizes the three-dimensional plane-wave component. However, to satisfy Helmholz equation the magnitude of $\mathbf{k}$ is constrained such that $k=2\pi f/c$, where c is the velocity of light. Propagation in a uniform medium is characterized by the propagation operator

$$\Theta\psi\left(x,\boldsymbol{\rho}\right)=\iint\widehat{\psi}\left(x_0,\boldsymbol{\kappa}\right)\exp\{ik(\sqrt{1-\left(\kappa/k\right)^2}-1)\Delta x\}\exp\{i\boldsymbol{\kappa}\cdot\boldsymbol{\rho}\}\frac{d\boldsymbol{\kappa}}{\left(2\pi\right)^2}, \tag{3}$$

which advances the wavefield to $x+\Delta x$. Using k_x-1 references the phase to zero at the observation plane intercept at kx.

The second term in (1) introduces a phase perturbation, $k\Delta n\left(x,\boldsymbol{\rho}\right)\Delta x$, with $\Delta n\left(x,\boldsymbol{\rho}\right)$ representing the index of refraction variation. There is no compelling reason to approximate the propagation operator for simulations. However, the simplification afforded by the parabolic approximation, namely

$$k\sqrt{1-\left(\kappa/k\right)^2}-1)\Delta x \simeq \left(\kappa\rho_F\right)^2/2 \tag{4}$$

$$\rho_F = \sqrt{x/k}, \tag{5}$$

is essential for theoretical calculations. The parabolic wave equation (PWE) replaces the complete propagation operator with

$$\Theta\psi\left(x,\boldsymbol{\rho}\right)=\iint\widehat{\psi}\left(x_0,\boldsymbol{\kappa}\right)\exp\{i\left(\kappa\rho_F\right)^2\}\exp\{i\boldsymbol{\kappa}\cdot\boldsymbol{\rho}\}\frac{d\boldsymbol{\kappa}}{\left(2\pi\right)^2},$$

which is defined by the single variable, ρ_F. In Chapter 3 of Rino et. al [1] the development of field moment equations that exploit the parabolic approximation is reviewed. To complete the FPE/PWE development, we let

$$\begin{aligned}\Delta\phi\left(x,\boldsymbol{\rho}\right) &= k\Delta n\left(x,\boldsymbol{\rho}\right)\\ &\simeq -\left(2\pi K/f\right)\Delta N_e\left(x,\boldsymbol{\rho}\right),\end{aligned}\tag{6}$$

where $K=1.3454\times10^9$ m^2/s and $\Delta N_e\left(x,\boldsymbol{\rho}\right)$ is the local variation of the electron density. The approximation is applicable at VHF and higher frequencies.

In the ISM review mean and stochastic components of $\Delta N_e\left(x,\boldsymbol{\rho}\right)$ are identified. The PWE makes no distinction between refraction, diffraction, or ray tracing as demonstrated in Chapter 2 of Rino [1]. A more complete definition of the refractive index extends the frequency range to critical density where the refractive index becomes purely imaginary. In Rino et. al [5] configuration-space realizations were used to compare PWE integration to equivalent-phase-screen results. The equivalent phase screen approximation is surprisingly good for all path orientations relative to the magnetic field. In the remainder of this review, only equivalent phase-screen results will be considered.

2 Phase-Screen Theory

Phase-screen theory replaces the cumulative interaction along the propagation path with the path-integrated phase

$$\phi(\boldsymbol{\rho})=-\left(2\pi K/f\right)\int_0^L\Delta N_e(x,\boldsymbol{\rho})dx,\tag{7}$$

where L is the extent of the disturbed region. The background ionosphere is treated separately. The starting field

$$\psi\left(x_0,\boldsymbol{\rho}\right)=\exp\{i\phi(\boldsymbol{\rho})\},\tag{8}$$

initiates the phase-screen calculation. As discussed in Chapter 2 of [1], more representative starting fields can be used. However, when the disturbed region occupies only a small portion of the source to receiver propagation path, the plane-wave approximation captures the interaction with a curvature correction to the Fresnel scale and path loss. The field in a measurement plane at distance $x>x_0$ is generated by applying the PWE propagation operator with $\Delta x=x-x_0$.

2.1 Structure Measures

If $\phi(\boldsymbol{\rho})$ is a gaussian random process, the mutual coherence function (MCF) admits the following analytic representation:

$$\begin{aligned} \langle \psi(x_0, \boldsymbol{\rho}) \psi^*(x_0, \boldsymbol{\rho}') \rangle &= \exp\{-D(\Delta\boldsymbol{\rho})\} \quad (9) \\ D(\Delta\boldsymbol{\rho}) &= \left\langle (\phi(\boldsymbol{\rho}) - \phi(\boldsymbol{\rho}'))^2 \right\rangle / 2, \quad (10) \end{aligned}$$

The structure function $D(\Delta\boldsymbol{\rho})$ is formally equal to $1 - \langle \phi(\boldsymbol{\rho})\phi(\boldsymbol{\rho}') \rangle$. However, for the class of power-law processes of interest, the correlation function is not well defined at large separations. The spectral domain definition,

$$\begin{aligned} D(\Delta\boldsymbol{\rho}) &= \iint (1 - \cos(\boldsymbol{\kappa} \cdot \boldsymbol{\rho})) \Phi_{\Delta\phi}(\boldsymbol{\kappa}) \frac{d\boldsymbol{\kappa}}{(2\pi)^2} \\ &= 2 \iint \sin^2(\boldsymbol{\kappa} \cdot \boldsymbol{\rho}/2) \Phi_{\Delta\phi}(\boldsymbol{\kappa}) \frac{d\boldsymbol{\kappa}}{(2\pi)^2} \quad (11) \end{aligned}$$

is preferred. At small wavenumbers $\sin^2(2\boldsymbol{\kappa} \cdot \boldsymbol{\rho}) \propto \kappa^2$ mitigates a $\kappa^{-\gamma}$ inverse power-law SDF singularity, whereby the structure function is well defined for radial power-law indices up to 3. The autocorrelation function remains ill defined. The mutual coherence function is of particular interest because application of the propagation operator only affects the phase of the plane-wave components. Consequently, the MCF is propagation invariant.

Following the development in ISM, one can show that

$$\Phi_{\Delta\phi}(\boldsymbol{\kappa}) = (2\pi K/f) L \int \frac{\sin^2(\kappa_x L/2)}{(\kappa_x L/2)^2} \Phi_{\Delta N_e}(\kappa_x, \boldsymbol{\kappa}) \frac{d\kappa_x}{2\pi}. \quad (12)$$

The SDF of the field intensity as it propagates is the quantity of primary interest. The field intensity is defined as

$$I(x, \boldsymbol{\rho}) = |\psi(x, \boldsymbol{\rho})|^2.$$

In addition to an invariant MCF, it can be show that $\langle I(x, \boldsymbol{\rho}) \rangle = 1$. It follows that the scintillation index, which is denoted as $S4$ for historical reasons, is defined by the relation

$$S4^2 = \left\langle I(x, \boldsymbol{\rho})^2 \right\rangle - 1 \quad (13)$$

Higher order moments $\langle I(x, \boldsymbol{\rho})^m \rangle$ require knowledge of the probability density function, which are formally defined by the phase screen model. However, aside from the $S4$ relation, there are no analytitically tractable results.

In Chapter 3.4.2 of Rino [1] it was show that

$$\Phi_I(\boldsymbol{\kappa}) = \iint [\exp\{-g(\overline{\boldsymbol{\xi}}, \boldsymbol{\kappa}\rho_F^2)\} - 1] \exp\{i\boldsymbol{\kappa} \cdot \overline{\boldsymbol{\xi}}\} d\overline{\boldsymbol{\xi}} \quad (14)$$

where

$$g(\boldsymbol{\xi}, \boldsymbol{\eta}) = D_{\Delta\phi}(\boldsymbol{\xi}) + D_{\Delta\phi}(\boldsymbol{\eta}) - D_{\Delta\phi}(\boldsymbol{\xi} + \boldsymbol{\eta})/2 - D_{\Delta\phi}(\boldsymbol{\xi} - \boldsymbol{\eta})/2. \quad (15)$$

Subtracting 1 in the argument removes the singularity that supports $\langle I(x,\boldsymbol{\rho})\rangle = 1$, whereby

$$S4^2 = \iint \Phi_I(\boldsymbol{\kappa}) \frac{d\boldsymbol{\kappa}}{(2\pi)^2}. \tag{16}$$

Noting that $\boldsymbol{\eta} = \boldsymbol{\kappa}\rho_F^2$ is scale free, the scale free-variable $\overline{\boldsymbol{\xi}} = \boldsymbol{\xi}\rho_F^2$ is introduced. It follows that

$$\begin{aligned} \left[\Phi_I(\boldsymbol{\eta}/\rho_F^2)/\rho_F^2\right] &= \iint \left[\exp\{-g(\boldsymbol{\xi},\boldsymbol{\eta})\} - 1\right] \exp\{i\boldsymbol{\eta}\cdot\boldsymbol{\xi}\} d\boldsymbol{\xi} & (17) \\ g(\boldsymbol{\xi},\boldsymbol{\eta}) &= D_{\Delta\phi}\left(\boldsymbol{\xi}\rho_F^2\right) + D_{\Delta\phi}\left(\boldsymbol{\kappa}\rho_F^2\right) - \\ &\quad D_{\Delta\phi}\left(\boldsymbol{\xi}+\boldsymbol{\kappa}\right)/2 - D_{\Delta\phi}\left(\left(\boldsymbol{\xi}-\boldsymbol{\kappa}\right)\rho_F^2\right)/2 & (18) \end{aligned}$$

The connection to (12) follows from the spectral-domain form of $g(\boldsymbol{\xi},\boldsymbol{\eta})$:

$$g(\boldsymbol{\xi},\boldsymbol{\eta}) = \iint \sin^2\left(\boldsymbol{\xi}\cdot\boldsymbol{\varkappa}/2\right) \sin^2\left(\boldsymbol{\eta}\cdot\boldsymbol{\varkappa}/2\right) \left[\Phi_{\Delta\phi}\left(\boldsymbol{\varkappa}/\rho_F^2\right)/\rho_F^2\right] \frac{d\boldsymbol{\varkappa}}{(2\pi)^2}. \tag{19}$$

If $\Phi_{\Delta y\phi}(\boldsymbol{\kappa}) \propto \kappa^{-\nu}$ then $\left[\Phi_{\Delta y\phi}\left(\boldsymbol{\varkappa}/\rho_F^2\right)/\rho_F^2\right]$ depends only on the spectral index, ν. Moreover, at small wavenumbers $\sin^2\left(\boldsymbol{\xi}\cdot\boldsymbol{\varkappa}/2\right)\sin^2\left(\boldsymbol{\eta}\cdot\boldsymbol{\varkappa}/2\right) \propto \kappa^4$, which implies that the Fresnel filterering defined by the $\sin^2\left(\boldsymbol{\xi}\cdot\boldsymbol{\varkappa}/2\right)$ functions, suppresses the large-scale contributions such that the intensity SDF is well defined even if the MCF is not well defined. Finally, we note that upon approximating $\exp\{-g(\overline{\boldsymbol{\xi}},\boldsymbol{\kappa}\rho_F^2)\}$ by $1 - g(\overline{\boldsymbol{\xi}},\boldsymbol{\kappa}\rho_F^2)$, the well-known weak scatter result follows:

$$\Phi_I(\boldsymbol{\kappa}) \simeq 4\sin^2\left(\left(\kappa\rho_F\right)^2/2\right) \Phi_{\Delta\phi}(\boldsymbol{\kappa}). \tag{20}$$

The ramifications of the phase-screen model and its development are discussed in detail in Chapter 3 of Rino [1]. The problem has been that even though a complete strong-scatter phase-screen theory exists, the problem of carrying out the integrations implied by (12), (17), and (18), together with the additional integration required for diagnostic one-dimensional SDF calculation, is too computationally intensive for practical application. However, the fact that the structue is highly elongated suggests that two-dimensional propagation might well capture the essential relations. Following research that has evolved over the past several years, this seems to be the case. Supporting analysis is presented in [6] and Rino et. al [5].

2.2 Two-Dimensional Phase Screen Model

The two-dimensional phase-screen model is obtained formally by assuming that the structure variation is two dimensional. If the magnetic field is aligned with the z axis,

$$\Phi_{\Delta N_e}(\kappa_x,\boldsymbol{\kappa}) = \Phi_{\Delta N_e}(\kappa_x,\kappa_y)\, 2\pi\delta(\kappa_z) \tag{21}$$

whereby

$$\Phi_{\Delta\phi}\left(\kappa_y\right) = \left(2\pi K/f\right) L \int \frac{\sin^2(\kappa_x L/2)}{(\kappa_x L/2)^2} \Phi_{\Delta N_e}\left(\kappa_x, \kappa_y\right) \frac{d\kappa_x}{2\pi}, \tag{22}$$

with the κ_z variation replaced by $2\pi\delta\left(\kappa_z\right)$. To accommodate normalized units without introducing more definitions, we make the follow notation adjustments as determined by the context:

$$\begin{aligned} \Phi_{\Delta\phi}\left(\mu/\rho_F\right)/\rho_F &\rightarrow \Phi_{\Delta\phi}\left(\mu\right) \\ \Phi_I(\mu/\rho_F)/\rho_F &\rightarrow \Phi_I(\mu) \end{aligned}$$

The two-dimensional theory is developed in detail in Carrano and Rino [6]. The two-dimensional theory is completely defined by C_{pp}, p_1, p_2, and μ_0. In starts with the two-component model for the phase-screen SDF

$$\Phi_{\Delta\phi}\left(\mu\right) = C_{pp} \begin{cases} \mu^{-p_1} & \text{for } \mu \le \mu_0 \\ \mu_0^{p_2-p_1}\mu^{-p_2} & \text{for } \mu > \mu_0 \end{cases}. \tag{23}$$

Although p is used here to denote the power-law index, it is not strictly equal to the Equation (20) in ISM. This is a topic of additional research.

The intensity SDF is computed as follows:

$$g(\xi,\mu) = \int \sin^2\left(\xi\varkappa/2\right) \sin^2\left(\mu\varkappa/2\right) \Phi_{\Delta\phi}\left(\mu\right) \frac{d\varkappa}{2\pi} \tag{24}$$

$$\Phi_I(\mu) = 2\int_0^\infty \left[\exp\{-g(\xi,\mu)\} - 1\right] \exp\{i\mu\xi\} d\xi \tag{25}$$

$$S4^2 = 2\int_0^\infty \Phi_I(\mu) \frac{d\mu}{2\pi} \tag{26}$$

It as found that a universal strength parameter, formally equal to $\Phi_{\Delta\phi}\left(1\right)$,

$$U = C_{pp} \begin{cases} 1 & \text{for } \mu_0 \ge 1 \\ \mu_0^{p_2-p_1} & \text{for } \mu_0 < 1 \end{cases} \tag{27}$$

orders the data such that weak to moderate scatter prevails when $U < 1$ and strong scatter prevailed when $U > 1$. The code implementation of the two-dimensional theory will accept U, p_1, p_2, and μ_0 as defining parameters. The code will also compute the complex field SDF

$$D_{\mathrm{MCF}}\left(\mu\right) = 2\int_0^\infty \exp\{-D_{\Delta\phi}(\zeta)\} \cos\left(\zeta\mu\right) d\zeta, \tag{28}$$

where

$$D_{\Delta\phi}(\zeta) = \frac{1}{\pi}\int_0^\infty \sin^2\left(\zeta\mu/2\right) \Phi_{\Delta\phi}\left(\mu\right) d\mu, \tag{29}$$

is the phase structure function.

2.3 Phase Screen Simulation

A multi-frequency phase-screen simulator was developed for GNSS simulations. The model is described in Rino et. al [7]. The means of generating multi-frequency GNSS phase simulations is straightforward. To review the essential elements of the model, a phase-screen complex field realization starts with a phase realization,

$$\phi_n = \sum_{m=0}^{N-1} \sqrt{\Phi_\phi\left(m\Delta q\right)\Delta q/\left(2\pi\right)}\eta_m \exp\{-2\pi inm/N\}, \tag{30}$$

where η_m is a zero-mean random process with the Hermitian property $\eta_m = \mathrm{mod}(\eta_N^*, N)$, and the white-noise property $\langle \eta_m \eta_{m'}^* \rangle = \delta_{m-m'}$. Configuration-space realizations could be used as well, but the current implementation uses only the conventional method, (30). The two-component power-law model

$$\Phi_\phi\left(q\right) = C_p \left\{ \begin{array}{ll} q^{-p_1} & \text{for } q \le q_0 \\ q_0^{p_2-p_1} q^{-p_2} & \text{for } q > q_0 \end{array} \right. , \tag{31}$$

defines the phase SDF, $\Phi_\phi\left(q\right)$. An initiating field

$$\psi_0\left(n\Delta y\right) = \exp\{i\phi\left(n\Delta y\right)\}, \tag{32}$$

is propagated to an observation plane at distance x from the phase screen as follows:

$$\widehat{\psi}(0; m\Delta q) = \sum_{n=0}^{N-1} \psi_0\left(n\Delta y\right) \exp\left\{-2\pi inm/N\right\} \tag{33}$$

$$\psi\left(x; n\Delta y\right) = \frac{1}{N}\sum_{m=0}^{N-1} \widehat{\psi}(0; m\Delta q) \left[\exp\left\{-ik\left[1-\sqrt{1-\left(q/k\right)^2}\right]x\right\}\right] \exp\left\{2\pi ink/N\right\}. \tag{34}$$

3 Model Applications

A collection of MatLab utilities and supporting libraries have been developed to facilitate the applications of the two-dimensional theory and phase-scree simulations. The directory `\PhaseScreenScintillationModel` contains subdirectories with supporting documentation, libraries, and demonstration utilities. MatLab utilities in the subdirectory `\IspectrumDemoCodes` will accept defining parameters and generate $\Phi_I(\mu)$, $S4$, and $MCF_{\Delta\phi}(\mu)$. The results are independent of ρ_F, and effectively capture the μ range 0 to ∞. This is achieved with non-uniform sampling that can be interpolated to any desired μ range. To define a specific μ range for an application, we first note that structure definition necessarily applies to specified segments of finite length, Y. Uniformly

spaced samples are generated at dy increments such that $N = Y/dy$. The additional parameters, Y and dy or N define the resolved spatial frequency range. Following the usual discrete Fourier transform (DFT) convention,

$$\begin{aligned} -N\Delta q/2 &\leq q_n \leq (N-1)\Delta q/2 & (35)\\ \Delta q &= 2\pi/Y. & (36) \end{aligned}$$

Only the non-negative frequency range is needed because of the symmetry of the SDFs.

Time-series are generated by the motion of the propagation through to the structure. This leads to the following ROI space-to-time equivalence,

$$y - y_0 = v_{\text{eff}}(t - t_0). \tag{37}$$

Temporal frequency is referenced to the carrier frequency, whereby frequency displacements are formally Doppler shifts covering the Doppler frequency range

$$\begin{aligned} -N\Delta f_{\text{Dop}}/2 &\leq f_{\text{Dop}n} \leq (N-1)\Delta f_{\text{Dop}}/2 & (38)\\ \Delta f_{\text{Dop}} &= 2\pi/\left(N\Delta t\right). & (39) \end{aligned}$$

The relations among the unnormalized and normalized variables can be summarized as follows:

$$\begin{aligned} q_n &= 2\pi/v_{\text{eff}} f_{\text{Dop}n} & (40)\\ \mu_n &= q_n\rho_F & (41)\\ &= 2\pi\left(\rho_F/v_{\text{eff}}\right) f_{\text{Dop}n} & (42) \end{aligned}$$

3.1 Normalized Frequency Range

Either ρ_F or ρ_F/v_{eff} can be treated as scale factors that convert spatial or temporal frequencies to a normalized frequency range. Figure 1 shows the nonuniformly sampled calculations of $\Phi_I(\mu)$ (red) and $D_{\text{MCF}}(\mu)$ (green) generated by `Ispectrum Ispectrum` and `Dspectrum` for the parameters listed in the figure title. The values $\mu = \mu_m$ are non uniformly sampled to capture essentially the range $0 < \mu < \infty$ with interpolation. The value of ρ_F or ρ_F/v_{eff} is determined by the following maximization

$$\widehat{S}_4 = \max_{\uparrow\rho_F} \sum_{n=1}^{N} \Phi_I(q_n\rho_F)\frac{dq_n}{\pi}. \tag{43}$$

Two utilities, `q2mu and Doppler2mu`, will generate either ρ_F for a specified spatial frequency range or ρ_F/v_{eff} for a specified Doppler frequency range. The effective scale factors are chosen to capture the significant content of the theoretical SDF. As an example, the overlaid magenta curve in Figure 1 shows the uniformly sampled range corresponding to the specified Doppler range and

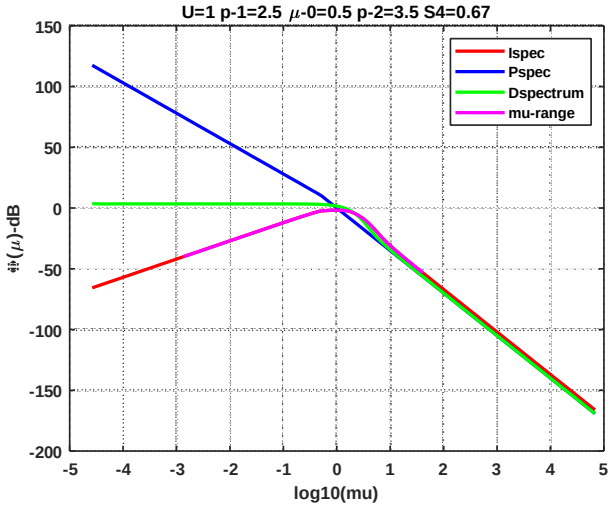

Figure 1: Red and green curves are from `Ispectrum`. Magenta intensiy SDF overlay is generated by interpolation to range generated by Doppler2mu. Blue curve is phase SDF.

sampling. For reference, the uniformly spaced defining phase SDF is shown in blue. The Fresnel scale determines propagation distance at which $\Phi_I(\mu)$ and $S4$ would be observed at a specified frequency. It also translates the normalized structure parameters to measures with specified units, namely

$$C_p = C_{pp}/\rho_F^{p_1-1} \quad (44)$$

$$q_0 = \mu_0/\rho_F^{p_1} \quad (45)$$

With the phase PSD and ρ_F/v_{eff} specified, it is straightforward to generate phase-sceen realizations with any desired sampling. The utility `GeneratePhaseScreenRealizationModel` can be used as a template for generating multi-frequency phase-screen realizations. The defaults are for the L1, L2, and L5 GPS frequencies. Defaulting the intput parameters will generate the Figures 1, 2, and 3. Figure 2 shows the dB intensity and phase realizations with the S4 indices listed.

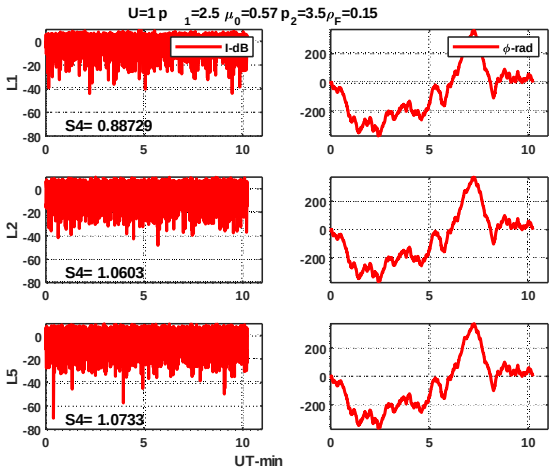

Figure 2: L1, L2, and L5 intensity and phase realizations extracted from the phase-screen complex field.

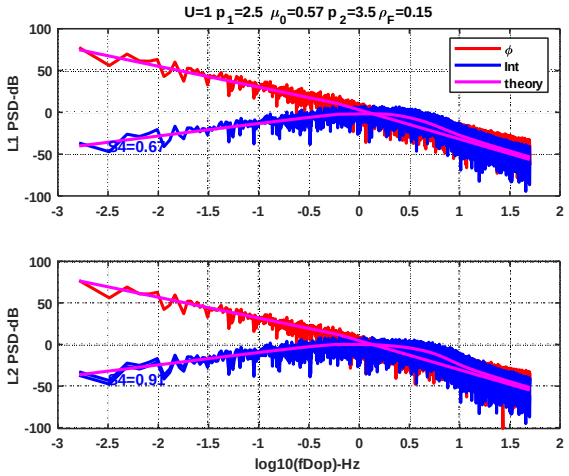

Figure 3: Measured L1 and L2 intensity (blue) and phase (red) SDFs. The magenta overlays are the theoretical results shown in Figure 2.

3.2 Phase Extraction

Extracting phase from a complex series starts with the *wrapped* phase defined by the arctangent operation.

$$W\{v_n\} = \arctan 2(\text{imag}(v_n), \text{real}(v_n)). \tag{46}$$

A standard unwrap utility will generate a phase sequence. However, we recently discovered the even though the phase realization is critically sampled, the unwrapping utility requires single-sample phase changes to be less than 2π. Otherwise, there are residual phase jumps in the reconstructed phase. The phenomenon is described and demonstrated in the paper [8] together with a modified reconstrjuction algorithm that uses successive interpolation to extract an error free phase reconstruction, [phase,nint]=ConstructPhase(psi). If the complex field, psi, has dimension N, the reconstructed phase has dimension $nint * N$, where $nint$ is the interpolation. To recover the corrected phase at the original sampling $phase = phase(1 : nint : nint * N)$. Examples can be found in [8].

References

[1] Charles L. Rino. *The Theory of Scinillation with Applications in Remote Sensing*. Wiley, 2011.

[2] C. Rino, K. Groves, C. Carrano J. Gunter, and R. Parris. Digital signal processing for ionospheric propagation diagnostics. *Radio Sci.*, 50, 2014. doi:10.1002/2014RS005625.

[3] K. G. Budden. The amplitude fluctuations of the radio wave scattered from a thick ionospheric layer with weak irregularities. *J. Atmos. and Terr. Phys.*, 27:155–172, 1964.

[4] B. H. Briggs and I. A. Parkin. On the variation of radio star and satellite scintillations with zenith angle. *J. Atmos. and Terr. Phys.*, 25:339–365, 1962.

[5] C. Rino, C. Carrano, and K. Groves. Wave propagation in extended highly anisotropic media. *Radio Science*, 2019. doi:10.1029/2019RS006793.

[6] C. Carrano and C. Rino. A theory of scintillation for two-component power law irregularity spectra: Overview and numerical results. *Radio Science*, 51:789âĂŞ813, 2016. doi:10.1002/2015RS005903.

[7] C. Rino, B. Briestch, Yu Morton, Yu Jiao, D. Xu, and C. Carrano. A compact multifrequency gnss scintillation model. *Institute of Navigation Journal*, pages 1–7, 2018. doi: 10.1002/navi.263.

[8] C. Rino, B. Brietsch, Yu Morton, Dongyang Xu, and C. Carrano. Gnss signal phase, tec, and phase scintillation. *Institute of Navigation Journal*, 2020. Submitted for Publication.

4